UNIVERSITY OF LEEDS

This is a repository copy of *Nested-Nanobubbles for Ultrasound Triggered Drug Release*.

White Rose Research Online URL for this paper:
https://eprints.whiterose.ac.uk/161651/

Version: Accepted Version

Article:

Nested-Nanobubbles for Ultrasound Triggered Drug Release

Damien V. B. Batchelor[1], Radwa H. Abou-Saleh[1,2], P. Louise Coletta[3], James. R. McLaughlan[3,4] Sally A. Peyman[1,3], Stephen D. Evans*[1].

[1]Department of Physics and Astronomy, University of Leeds, Leeds, UK, [2] Department of Physics, Mansoura University, Mansoura, Egypt, [3]Leeds Institute of Medical Research, Wellcome Trust Brenner Building, St James' University Hospital, Leeds, UK, [4]School of Electronic and Electrical Engineering, University of Leeds, Leeds, UK

KEYWORDS: nanobubbles, liposome, ultrasound, drug delivery, triggered release, droplets

ABSTRACT

Due to their size (1-10 μm) microbubble-based drug delivery agents suffer from confinement to the vasculature, limiting tumour penetration and potentially reducing drug efficacy. Nanobubbles (NBs) have emerged as promising candidates for ultrasound triggered drug delivery, due to their small size allowing drug delivery complexes to take advantage of the enhanced permeability and retention effect. In this study we describe a simple method for production of Nested-NBs, by encapsulation of NBs (~ 100 nm) within drug loaded liposomes. This method combines the efficient and well-established drug loading capabilities of liposomes, whilst utilizing NBs as an acoustic trigger for drug release. Encapsulation was characterized using Transmission Electron

Microscopy with an encapsulation efficiency of 22 ± 2 %. Nested-NBs demonstrated echogenicity using diagnostic B-mode imaging and acoustic emissions were monitored during high intensity focused ultrasound (HIFU) in addition to monitoring of model drug release. Results showed that although the encapsulated NBs were destroyed by pulsed HIFU (peak negative pressure 1.54 – 4.83 MPa), signified by loss of echogenicity and detection of inertial cavitation, no model drug release was observed. Changing modality to continuous wave (CW) HIFU produced release across a range of peak negative pressures (2.01 – 3.90 MPa), likely due to a synergistic effect of mechanical and increased thermal stimuli. Due to this, we predict that our NBs contain a mixed population of both gaseous and liquid core particles, which upon CW HIFU undergo rapid phase conversion, triggering liposomal drug release. This hypothesis was investigated using previously described models to predict the existence of droplets and their phase change potential and the ability of this phase change to induce liposomal drug release.

1 Introduction

Chemotherapy, in combination with surgery or radiotherapy, is one of the primary treatment methods for malignant tumors and can significantly increase patient survival rates. However, treatment efficacy is currently limited by the negative side-effects and drug resistance present during systemic delivery. [1] The ability to target and locally deliver chemotherapeutics would help to reduce toxic side-effects, but also increase drug efficacy and treatment effectiveness. Drug-loaded liposomes, such as Doxil and Onivyde, reduce the exposure of healthy tissues to drug and are currently approved for clinical use. However, due to the lack of a triggered release mechanism in addition to hepatic and renal clearance, drug efficacy is not maximised.[2] Methods for triggering release using mechanical and thermal approaches such as ultrasound (US) [3] and

near-infrared lasers [4] are currently being developed for improving controlled local release. The use of US is appealing due to its wide-spread availability, non-invasive nature and potential for image guidance during treatment. US imaging utilizes high-frequency sound waves that propagate through tissue and the back-scattered waves are used to construct an image. Microbubbles (MBs) are commonly used as ultrasound contrast agents (UCAs) due to their high acoustic-impedance mismatch with surrounding tissue, whilst their size of 1 - 10 μm allows facile circulation through the vasculature. MB stability is enhanced by using high molecular weight, low solubility gases such as perfluorocarbons [5] or Sulphur Hexafluoride (SF_6) [6] as well as a coating, typically a phospholipid monolayer, protein or polymer [7–9]. Recently, research has focused on the potential use of MBs as theranostic agents. [10,11] MBs driven by an US field can enhance sonoporation in cell membranes, which has been shown to increase drug uptake.[9,12–14] Therapeutics can be incorporated with MBs in multiple ways including therapeutic gas [15], direct attachment of drugs to the lipid shell [16] and attachment of drug-filled liposomes [17–19] which can be released by increasing US intensity. Surface functionalization of the MB shells can be used to provide molecular targeting [17] and improved stealth properties. [20] However, to increase tumor bio-distribution and take advantage of the enhanced permeation and retention (EPR) effect provided by the leaky vasculature, the drug delivery complex should be < 400 nm. [21,22] As such, nanobubbles (NBs), sub-micron bubbles typically 200 – 600 nm in diameter [23,24], are an attractive prospect for drug delivery and have shown increased tumor accumulation and retention compared to MBs. [25,26] We have previously reported the production and characterization of NBs using microfluidics [27] with others using methods such as mechanical agitation and sonication.[28–30] The inverse relationship between Laplace pressure and bubble radius leads to predicted lifetimes on the order of microseconds. [31,32] In spite of this NBs have demonstrated remarkable

stability [27,33,34] which has raised speculation as to their physical state and the nature of stabilization. [31,32,35,36] NBs provide US contrast enhancement at frequencies below their resonance and hence provide promise for diagnostic use. [37,38] Further, they have also been used for the delivery of therapeutics either by co-delivery [39] or by direct incorporation of their payload. [26,29,40,41]

In this paper we introduce Nested-Nanobubbles (Nested-NBs) as sub-micron US triggered drug delivery vehicles. Nested-NBs consist of an outer liposomal shell containing both the encapsulated drug payload and one or more NBs that can act as internal nuclei for an US triggered release. The NBs were produced using microfluidics [27] and encapsulated together with calcein within liposomes via thin film rehydration. Encapsulation of NBs was demonstrated using Transmission Electron Microscopy (TEM) and Nested-NBs echogenicity characterized using clinical B-mode ultrasound imaging, which subsequently decreased after High Intensity Focused Ultrasound (HIFU) trigger. Nested-NBs were loaded with calcein to act as a model drug and for pulsed HIFU exposures, no release was observed. However, the use of a continuous wave US exposure triggered calcein release for free field peak negative pressure ranging from 2.01 ± 0.10 MPa to 3.90 ± 0.10 MPa. Our results suggest that the release mechanism is a synergistic effect of mechanical and thermal stimuli and that our NB populations contain a mixture of particles both their gaseous and liquid phases, the latter of which undergo a low-pressure phase-change. This drug delivery vehicle provides the acoustic diagnostic properties of NBs combined with the therapeutic advantages offered by liposomes and with the additional benefit of an external triggered release mechanism.

2 Methods

2.1 Microfluidic Production of Nano- and Microbubbles

Nano- and microbubbles were prepared from a mixture of DPPC (1,2-dipalmitoyl-sn-glycero-3-phosphocholine) and DPSE-PEG2000 (1,2-distearoyl-sn-glycero-3-phosphoethanolamine-N-[methoxy(polyethylene glycol)-2000]) in a 95:5 molar ratio and a total lipid concentration of 2 mg/mL (Avanti Polar Lipids, AL, US). Lipids were dissolved in a 1:1 mixture of Chloroform and Methanol and dried under Nitrogen to remove the solvent and subsequently resuspended in PBS solution containing 1 % (v/v) glycerol. The lipid solution was then combined with C_4F_{10} (PFB) gas in a multiplexed microspray microfluidic device for bubble production as described in Peyman et al. [27]

2.2 Nanobubble Isolation

NBs were passively isolated from MBs via flotation due intrinsic MB buoyancy. A spherical bubble in a medium has an ascension velocity, described by the Hadamard-Rybczynski equation (Equation 1).[42] For a PFB bubble with radius of 1 μm it would take 47 minutes to travel 1 cm. For a bubble in the same medium with diameter of 150 nm it would take 840 minutes to travel the same distance and as such can be regarded as neutrally buoyant. After 1 hour, a syringe and fine needle was used to remove NB sample from the bottom of the vial and subsequently filtered through 800 nm PTFE membrane to remove any large bubbles.

$$U = \frac{2gR^2\Delta\rho}{3\mu}\frac{\mu + \mu'}{2\mu + 3\mu'}$$

$$(1)$$

Where U is ascension velocity, g is gravitational acceleration (9.81 ms^{-1}), R is radius, $\Delta\rho$ is difference in density between the medium and the core, μ is dynamic viscosity of water (8.9 x 10^{-4} Pa s) , μ' is dynamic viscosity of C_4F_{10} (1.2 x 10^{-5} Pa s).

2.3 Nanobubble size and concentration determination

Nanoparticle Tracking Analysis (NTA). Single particle tracking was used to analyse NB populations using NanoSight Nanoparticle Tracking Analysis (NanoSight NS300, Malvern Panalytical, UK). Samples were illuminated with a 488 nm laser and individual particles tracked using NTA 3.3 software. Samples were diluted 1:1000 in PBS prior to measurement and measurements repeated in triplicate.

Resonant Mass Measurement (RMM). Resonant mass measurement (Archimedes, Malvern Panalytical, UK) was used to demonstrate and analyze populations of positively buoyant (bubbles) and negatively buoyant particles in NB solutions. Archimedes was equipped with a MicroH sensor capable of measurement of particle diameters of between 150 – 5000 nm and pre-calibrated with 1 μm polystyrene beads (ThermoScientific Microsphere Size Standards 4010A) Samples were diluted 1:500 in PBS prior to measurements. During the measurement, NB sample was loaded initially for 120 seconds and analyzed at pressures of 3, 2 and 3 psi for sample, reference and experiment values. Limit of detection was set to 25 mHz to provide consistency for all measurements. Particle densities were set to 0.0112 and 1.3 g/mL for positively buoyant and negatively buoyant particles respectively, corresponding to the density of PFB gas and lipid vesicles.[43]

2.4 Liposome and Nested-Nanobubble Production

A combination of DSPC, Cholesterol and DSPE-PEG2000 were dried under Nitrogen in round bottom flasks in a 63:32:5 molar ratio at a total lipid concentration of 15 mg/mL The lipid film was resuspended in either PBS buffer for liposome production or with NBs at stock concentration for Nested-NB production and rehydrated via stirring for 1 hour. For calcein loading, solution pH adjusted using 10 M NaOH to pH 10.5 and calcein added to a final concentration of 100 mM prior to rehydration. Rehydrated lipid solution was homogenized via

extrusion by passing through a 400 nm PTFE membrane. Free calcein and NBs were removed via centrifugation at 17,000 g for 20 minutes, washed with PBS and centrifugation and washing were repeated once. (Scheme 1)
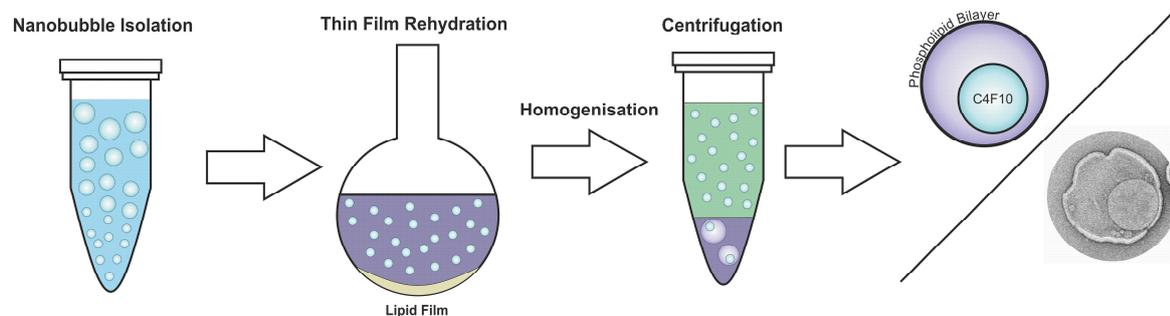
Scheme 1. Preparation of Nested-NBs by isolation of NBs via buoyancy, thin film rehydration of a lipid film and cleaning via centrifugation.

2.5   Transmission Electron Microscopy

For Transmission Electron Microscopy (TEM), samples were prepared in a phosphate free buffer and 5 uL of sample pipetted onto glow discharged carbon grids. After 30 seconds incubation, sample was washed with buffer and 5 uL of 1 % uranyl acetate added for 30 seconds, then removed and left to air dry. Images were taken at a range of magnifications ranging from 11,000 to 46,000 x using a FEI T12 transmission electron microscope (FEI Tecnai T12, USA). Images were analyzed manually using ImageJ (NIH, US) to determine particle diameter.

2.6   Encapsulation and Release Efficiency

Fluorescence spectroscopy was used to quantify the release of calcein from within Nested-NBs and liposomes from ultrasound exposures. Due to the high concentration of encapsulated calcein within the liposomes, calcein fluorescence was initially quenched. However, when released from the liposome into the bulk medium, calcein concentration decreases and subsequently unquenches. Nested-NB and liposome samples were diluted 1:25 in PBS to increase sensitivity of the fluorescence assay. Sample fluorescence was measured using a microplate reader

(SpectraMax M2E, Molecular Devices, US) with excitation and emission wavelength of 460 and 515 nm respectively. Nested-NB and LS sample fluorescence was measured for non-exposed samples (negative control), exposed sample and samples lysed with 0.1 % Triton-X (positive control) to calculate the percentage of calcein released from the sample. Percentage release was calculated by Equation 2, where $FL_{HIFU}, FL_{+control}$ and $FL_{-control}$ are fluorescence intensities for HIFU exposed, positive and negative control samples respectively.

$$\% \text{ Release} = 100 \text{ x } (FL_{HIFU} - FL_{-\text{ control}})/(FL_{+control} - FL_{-control}) \qquad (2)$$

2.7 Ultrasound Imaging

B-mode diagnostic US images of NB and Nested-NB populations were produced using a 3-8 MHz linear array probe (V-Scan, GE Healthcare, IL, US). Samples were imaged in a wall-less agar flow phantom, produced by mixing 3 % by mass agar and 8 % by mass glycerol with degassed water [44]. The mixture was heated in a microwave and manually stirred intermittently until a homogenous solution was produced. The mixture was poured into a 3D printed mould containing a 4 mm outer diameter tube and left to cool. The tube was removed after the agar had set and Luer lock fittings attached for sample loading. Mean grayscale intensity of B-mode images were calculated in the region of interest using MATLAB (Mathworks Inc, US).

2.8 High Intensity Focused Ultrasound (HIFU) and Passive Cavitation Detection (PCD)

A single element High Intensity Focused Ultrasound (HIFU) transducer was used for US mediated NB destruction. A 1.1 MHz center frequency HIFU transducer (H-102, Sonic Concepts, US) was used for all HIFU experiments. The transducer was connected to a +55 dB power amplifier (A300, E&I Ltd, US) via an impedance matching circuit. A computer-controlled function generator (33220A, Agilent, US) was used to provide sinusoidal burst cycles to the transducer. Free field pressure was measured using a membrane hydrophone (Precision Acoustic

Ltd, Dorchester, UK) with a 400 μm sensitive element, calibrated by the National Physics Laboratory (Middlesex, UK). [45] All pressures stated are based from their free field calibrations with errors of ± 0.1 MPa. The HIFU transducer was coupled to the sample using a coupling cone containing degassed MilliQ water. A TTL digital delay pulse generator (9524, Quantum Composers, MT, USA) was used to synchronize the HIFU pulse and data acquisition system. A broadband focused detection (Y-102, Sonic Concepts, WA, USA) was positioned in the central aperture of the HIFU transducer and co-aligned with its focal region. It was connected to a 5 MHz high pass filter (Allen Avionics,US) and a 40 dB pre-amplifier (Spectrum GmbH,Germany). A 14-bit data acquisition (DAQ) card (M4i.4420-x8, Spectrum GmbH, Germany) was used to record acoustic emissions. A desktop PC was used to control all hardware and post-processing using MATLAB. For each HIFU pulse, 163 μs of cavitation data was recorded and Fast Fourier Transformed into the frequency domain. Frequency data was comb filtered to either remove harmonics, leaving only broadband emissions. [46] Additionally, the inverse comb filter was applied to remove broadband emissions, leaving only ultraharmonic emissions. Data was recorded for 0.5 s either side of the 5 s HIFU exposure with initial values before HIFU used as a noise baseline. To maximize the magnitude of acoustic emissions, the concentration of Nested-NBs and Liposomes were maintained as high as possible whilst remaining constant between the two samples at 1.56×10^{11} particles/mL.

3 Results and Discussion

3.1 Nanobubble Characterisation

NBs were produced using the micro-fluidic micro-spray approach and separated from the microbubbles by floatation of the microbubble and collection of the sub-natent. NB populations were characterised using three separate techniques; Nanoparticle Tracking Analysis (NTA),

Resonance Mass Measurement (RMM) and Transmission Electron Microscopy (TEM). Using NTA the NB concentration and size, measured across five sample preparations, were found to be 5.79 ± 0.66 x 10^{11} /mL, with a modal size of 106 ± 4 nm (Figure 1a). NBs were also analysed using RMM (Figure 1b) a technique that can distinguish between positively buoyant particles (i.e. ones that are less dense than the solution) and negatively buoyant particles (i.e. denser than the solution). RMM also measures the size and concentration of the positively and negatively buoyant particles. The average concentrations and sizes measured from 3 separate samples were found to be 1.17 ± 0.68 x 10^9 /mL and 3.54 ± 1.20 x 10^9 /mL with respective modal sizes of 212 ± 12 nm and 321 ± 32 nm for the positively and negatively buoyant particles respectively (Figure 1b). The negatively buoyant population likely consists of a combination of lipid particles that were not converted into bubbles as well as potentially containing PFB droplets, that due to their small size have condensed from a gas into liquid PFB droplets. However, the limit of detection of the RMM system was around 200 nm, thus failing to determine the nature of the particles making-up the largest contribution to the NTA data circa 100 nm. Additionally, NBs were imaged using TEM and their size distribution analysed. A total of 252 NBs across 31 images were counted and their sizes analysed, demonstrating a log-normal distribution with a size of 120 ± 48 nm (Figure 1c), with a representative TEM image is shown in Figure 1d. A small proportion of < 100 nm particles were measured via TEM, again likely to be lipid vesicles or PFB droplets below the detection threshold for both NTA and RMM analysis. Comparison between the three measurement techniques used show agreement between both NTA and TEM results, in terms of their respective modal sizes and the population distributions. However, for RMM, the limit of detection is higher than that of the modal particle size, thus a large proportion of the NB

population is likely missing. Notwithstanding this, RMM is still useful for confirming the presence of sub-micron bubbles, as opposed to just particles.
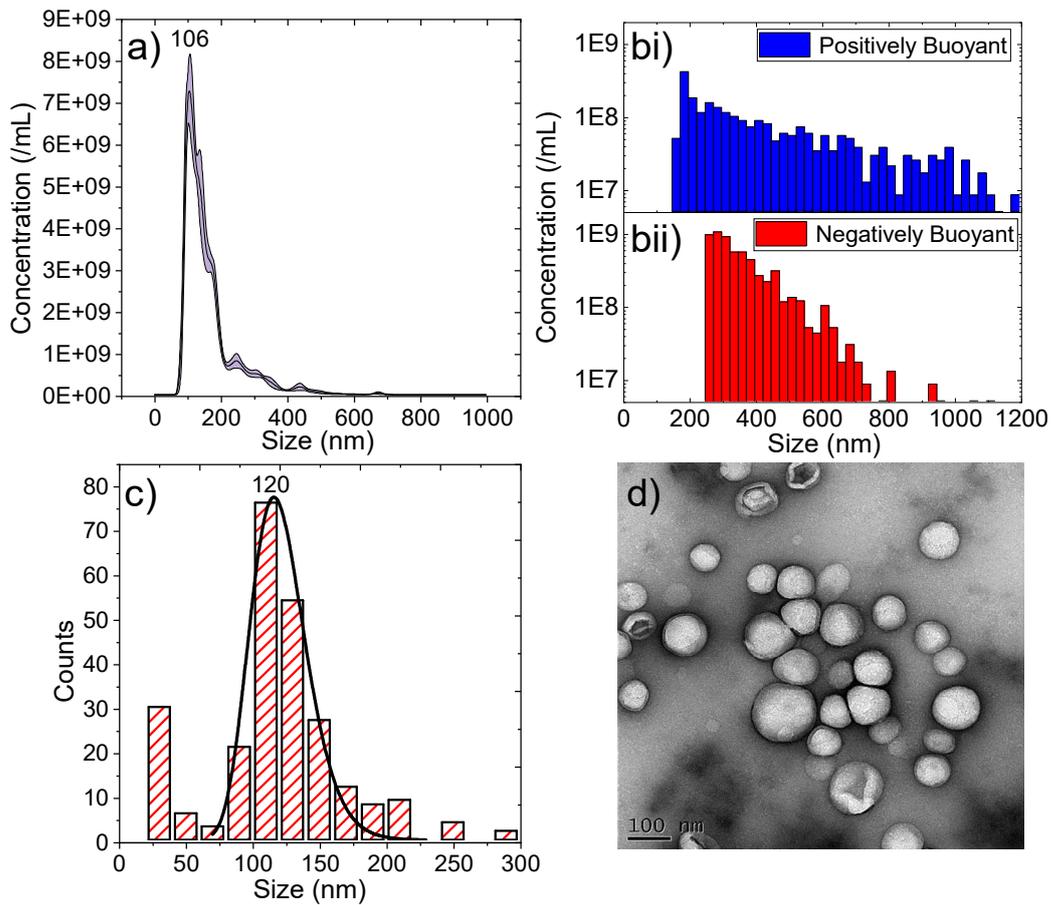
Figure 1. Characterisation of Nanobubbles using (a) Nanoparticle Tracking Analysis (NTA), (b) Resonant Mass Measurement (RMM) showing both (bi) Positively and (bii) Negatively buoyant particles and (c) transmission electron microscopy (TEM) with a representative image shown in (d).

NBs were imaged using B-mode imaging (3 - 8 MHz Broadband, Linear Array, MI = 0.8) using a flow-phantom to assess their echogenicity at clinically relevant imaging parameters. NB

concentration was measured via NTA and diluted to concentrations of ~ 10^9 – 10^{11} NBs/mL^{-1} to determine contrast enhancement across a range of concentrations. Mean Grayscale Intensity (MGI) of the B-mode images was measured in the region of interest (ROI) of the flow phantom (as shown in Figure 2ai) for each concentration and showed a linear increase in MGI with increasing concentration (Figure 2aii). It is also notable that the MI used for this experiment was larger than is typically used for micron scale UCAs (< 0.3), as greater than this typically induces microbubble destruction. However, NBs were stable during imaging experiments.

NBs were also exposed to high intensity focused ultrasound (HIFU) and the B-mode MGI measured prior to and post-exposure, to determine whether NB destruction had been achieved. The peak negative pressure (PNP) was varied between 1.06 – 6.75 MPa using a PRF of 1 kHz and 1 % duty cycle for a total of 5 seconds. MGI decreased exponentially with increasing pressure reaching a minimum MGI after exposure at 4.83 MPa (Figure 2b). Nanobubble destruction was also demonstrated using RMM, where positively buoyant particle concentration decreased by an order of magnitude, from 4.38 x 10^8 NBs/mL to 3.24 x 10^7 NBs/mL after HIFU exposure, whilst the negatively buoyant particle concentration remained unchanged (Figure 2c). Full population distributions before and after HIFU exposure are shown in Figure S1.
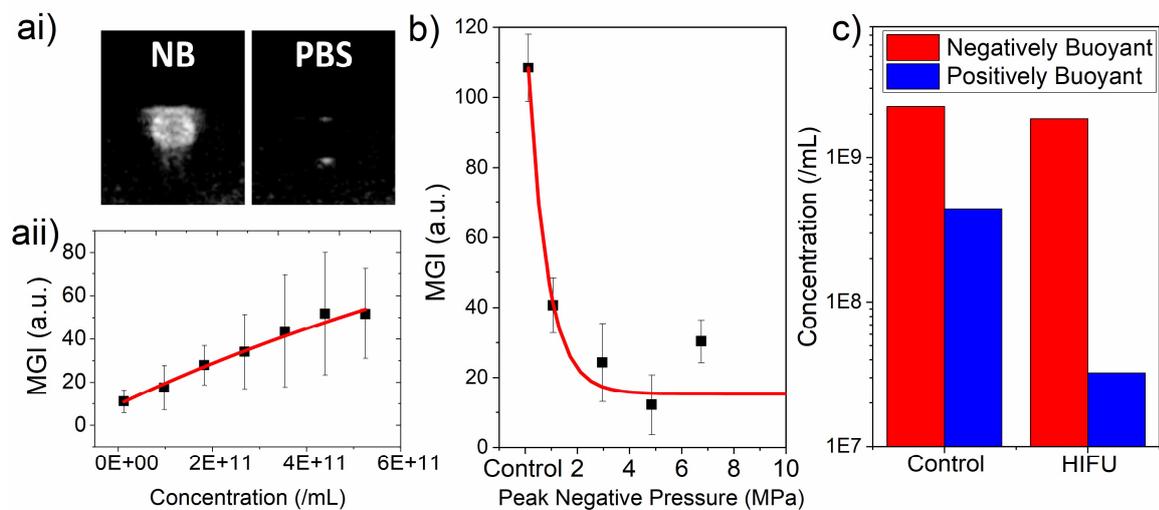
Figure 2. (ai) Representative clinical frequency B-mode (3-8 MHz Linear Array, MI = 0.8) images of NBs and PBS in a flow phantom and (aii) change in Mean Grayscale Intensity (MGI) for NBs with varying concentration. (b) MGI of B-mode images of NB sample after application of high intensity focused ultrasound (HIFU) with varying PNP. (c) Concentration of negatively buoyant and positively buoyant particles before and after HIFU exposure at PNP of 4.83 MPa with 1 % duty cycle, measured via RMM.

3.2 Nested-NB Production and Characterisation

Nested-NBs were produced by passive encapsulation of the NBs inside phospholipid liposomes. Calcein loaded at a concentration to give self-quenching was also encapsulated to simulate a model small molecule drug. After encapsulation, free calcein and small particles (< 200 nm), believed to be a combination of both un-encapsulated NBs and empty liposomes, were removed by centrifugation, as described in Section 2.4. The population distribution of the Nested-NBs post-cleaning is shown in Figure 3a. After cleaning Nested-NBs mean size increased from 182.6 ± 0.2 nm to 318.9 ± 7.1 nm and there was a concomitant decrease in concentration from $1.82 \pm 0.09 \times 10^{12}$ particles/mL to $2.45 \pm 0.10 \times 10^{11}$ particles/mL (Figure

13

S2). Additionally, after cleaning the mean grayscale intensity of B-mode images of Nested-NBs decreased from 30.5 ± 1.9 to 11.3 ± 0.7 as would be expected with the removal of free NBs (Figure S3).

The efficiency of NB encapsulation, within Nested-NBs, was determined using TEM. A total of 124 individual liposomes were analysed across 38 images, with $22 \pm 2\%$ of liposomes encapsulating single or multiple NBs. On average, each Nested-NB contained 1.29 ± 0.01 NBs.
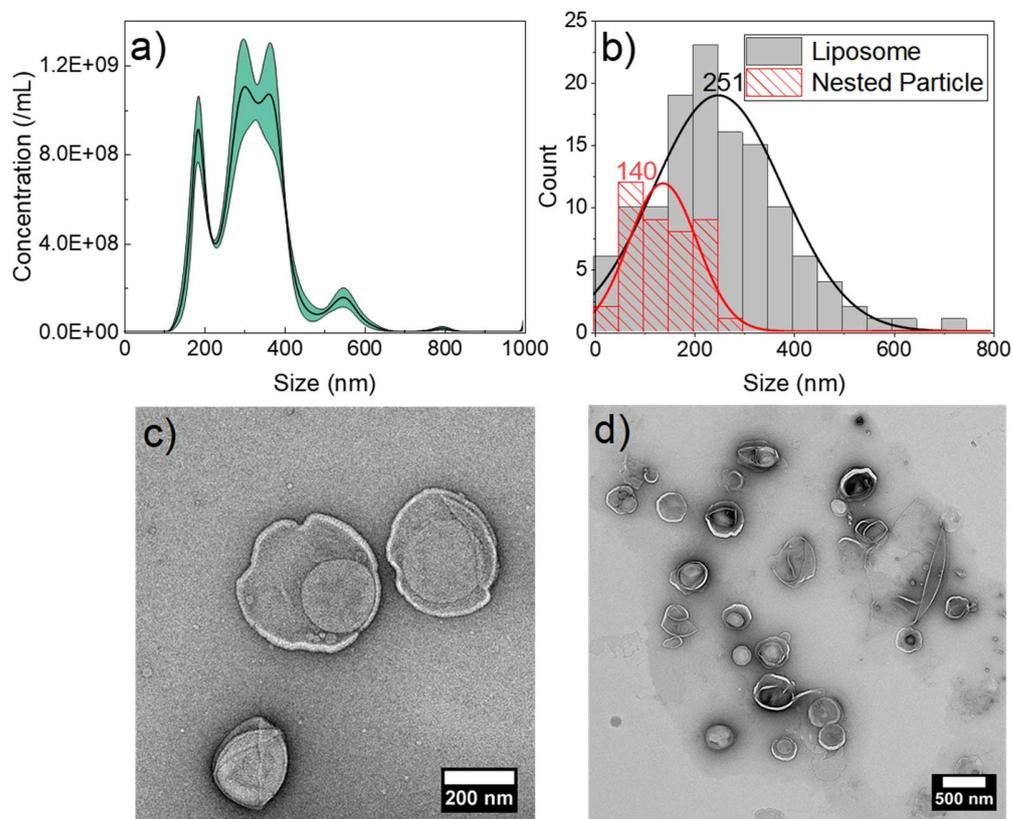
Figure 3. Nested-NB population distribution measured by (a) Nanoparticle Tracking Analysis and (b) Transmission Electron (TEM) microscopy, showing distribution for both the nested NB and the encapsulating liposome. (c) and (d): Representative TEM images of Nested-NBs showing two individual Nested-NBs and a larger field of view respectively.

Nested-NB size distribution measured via TEM is shown in Figure 3b, with populations for both their outer liposomal shell and encapsulated NBs analysed. Representative images are shown in (c) and (d), demonstrating clear encapsulation of a nesting particle within an outer liposomal shell. Population distributions followed a normal distribution with modal sizes of nesting particles and liposomes at 140 ± 69 nm and of 251 ± 130 nm respectively.

3.3 Ultrasound Triggered Release

Nested-NBs were exposed to HIFU to provide a mechanism for triggered NB destruction and subsequent payload release. Initially, Nested-NBs and Liposome only controls were insonated at free-field PNPs of 1.54, 2.96 and 4.83 MPa for a total of 5 seconds with duty cycles of either 1 or 50 %. Release profiles are shown in Figure 4a and 4b respectively. At these exposure parameters, no significant calcein release was observed from Nested-NBs compared to liposome only controls. To determine whether these exposures were inducing destruction of the encapsulated NBs, Nested-NBs were imaged using B-mode ultrasound before and after HIFU exposure. Nested-NBs initially demonstrated echogenicity, which after insonation at 4.83 MPa at 50 % duty cycle decreased by 92.4 ± 5.6 % from 60.3 ± 2.4 to 4.6 ± 0.8, suggesting NB destruction (Figure 4b inset).
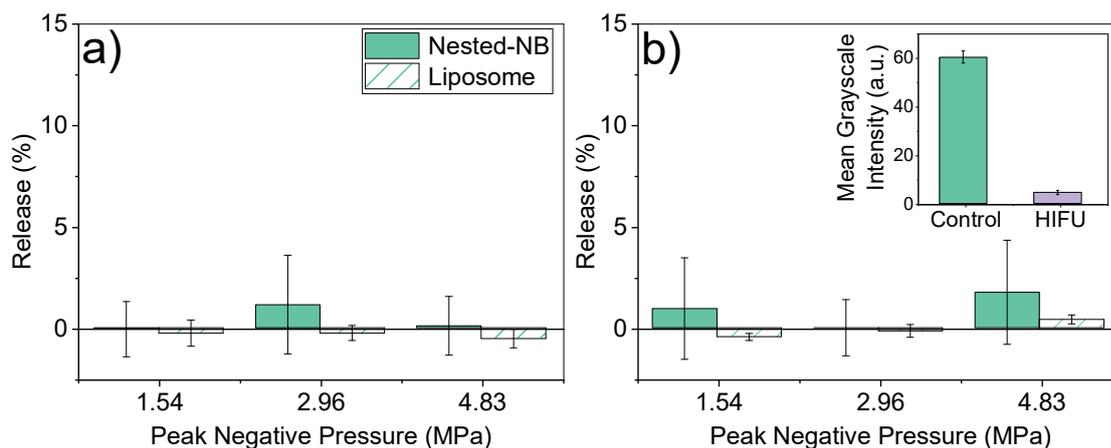
Figure 4. Release profiles for Nested-NBs and Liposome controls after ultrasound exposure at PNPs ranging from 1.54 MPa to 4.83 MPa at (a) 1 % Duty Cycle and (b) 50 % Duty Cycle. Inset: Mean grayscale intensity of B-mode imaging of Nested-NBs before and after HIFU exposure at 4.83 MPa at 50 % duty cycle.

The lack of observed release from HIFU mediated NB destruction led us to further investigate the interaction between Nested-NBs and the applied HIFU field. Passive cavitation detection was used to observe acoustic emissions during insonation. Nested-NB, liposome and PBS samples were each exposed to HIFU, at the previously described parameters. Acoustic emissions were converted into the frequency domain by Fast Fourier Transform and the magnitude of the broadband noise and ultra-harmonic emissions were determined to quantify the occurrence of inertial cavitation (bubble destruction) and stable cavitation (bubble oscillation). Due to the high PNP, NB destruction was expected to occur during the initial pulse cycles of the HIFU exposure. To quantify the change in the magnitude of acoustic emissions over time, broadband and ultra-harmonic emissions were cumulatively integrated with increasing pulse number and then normalised per pulse. Full temporal emissions for the whole exposure duration are shown in Figure S4. For both broadband (Figure 5a) and ultra-harmonic (Figure 5b) emissions, Nested-NBs demonstrate increased activity at the beginning of the exposure which decreased with

16

increasing pulse number to the value found for non-acoustically active liposomes. This suggests that the NBs present initially in the Nested-NB sample provide an increase in both broadband and harmonic emissions, as NBs undergo stable and inertial cavitation. As the HIFU exposure progresses, the broadband and harmonic emissions decrease until eventually by the end of the exposure the Nested-NB and liposome samples are indistinguishable from each other, with no NBs remaining. This is also in agreement with the near total loss of contrast shown by B-mode imaging (Figure 4b). Both Nested-NB and liposome samples demonstrated increased broadband and harmonic emissions compared to a PBS control, likely due to non-acoustically active liposomes providing cavitation nuclei. The relatively high value of the PBS control can be
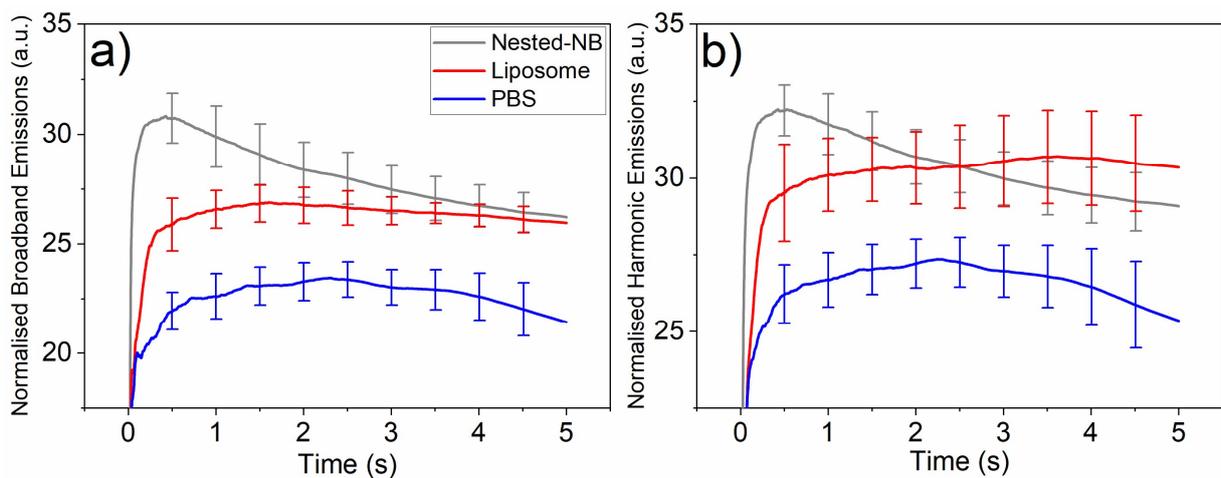
Figure 5. (a) Normalised Broadband Emissions and (b) Normalised Ultraharmonic Emissions measured using passive cavitation detection during insonation at 4.83 MPa and 50 % duty cycle for Nested-Nanobubbles, Liposomes and PBS samples. Data shows the acoustic emissions integrated over the number of pulses and then normalised per pulse.

attributed to a combination of both cavitation induced within the solution and acoustic reflections from the sample holder due to the relatively high PNP. Due to the lack of release observed from

Nested-NBs, it is possible that the detected inertial cavitation is occurring in the bulk solution, or that the encapsulated NBs are being destroyed but not capable of inducing drug release.

By changing the modality of the HIFU exposure from pulsed to continuous wave, we found that Nested-NBs showed calcein release for PNPs ranging from 2.01-3.90 MPa with an exposure time of 5 s. Figure 6a shows the release profiles for both Nested-NBs (solid) and Liposomes (hashed). The amount of release increased with increasing PNP for both samples up to a maximum Nested-NB release of 52.9 ± 10.3 % with a corresponding Liposome only release of 35.3 ± 9.2 %. Considering only the difference in release between Nested-NBs and Liposomes, a maximum difference of 26.2 ± 10.3 % was achieved at 2.96 MPa (Figure 6b). The difference in release is comparable to the encapsulation efficiency of NBs within Nested-NBs of 22 ± 2 %,
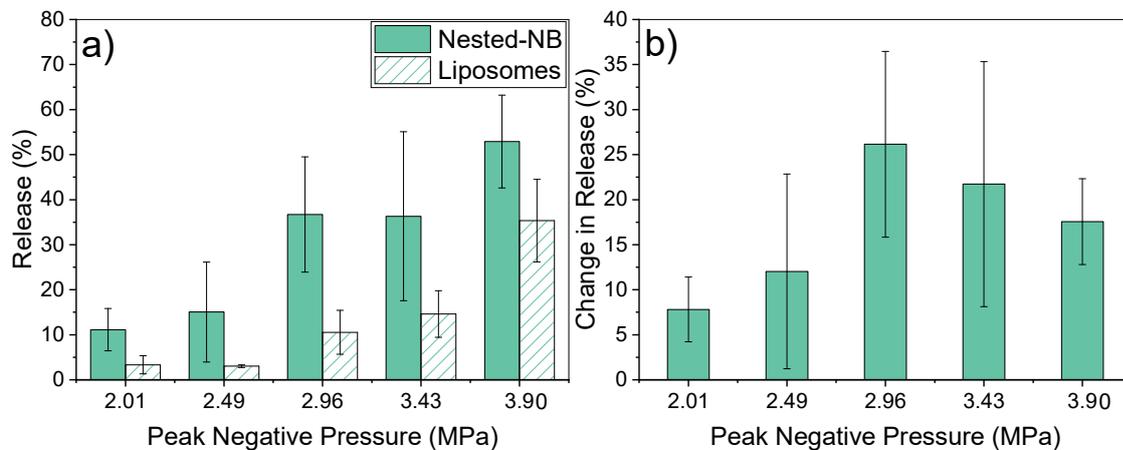
Figure 6. (a) Release profile of Nested-NBs and Liposome controls after continuous wave HIFU exposure at PNPs ranging from 2.01 – 3.90 MPa. (b) Difference in release of Nested-NBs compared to Liposome controls.

which would suggest that the efficacy of release of the Nested-NB is approaching 100 %. Increasing the PNP further led to a decrease in the difference in the release profiles. For the

Nested-NB sample, any release observed above that of the NB encapsulation efficiency, would likely be attributed to thermally induced release. Additionally, since no release was previously observed with pulsed HIFU exposures (Figure 4) the ability of continuous wave HIFU to induce release is helpful in identifying the release mechanism. Although NBs are present in the Nested-NB sample, RMM (Figure 1b) identified that 79 ± 4 % of the population concentration consists of negatively buoyant particles. As such, it is reasonable to assume that a similar proportion of encapsulated particles within the Nested-NBs would be negatively buoyant. Additionally, due to the modal size of encapsulated particles (~140 nm) being less than the limit of detection of RMM (~ 200 nm), the existence of bubbles of this size cannot be confirmed. Due to the inverse relationship between the Laplace pressure and bubble radius (Equation 3), in addition to the density of the PFB gas core used in our experiments, it is increasingly likely that as particle size decreases, a sub-population of PFB droplets would exist.

$$\Delta P = \frac{2\sigma}{r} \tag{3}$$

Where ΔP is pressure difference between inside and outside the particle, σ is surface tension of the interface and r is particle size.

The bulk boiling point of PFB is -1.7 ° C however, confinement into either a bubble or droplet will elevate this boiling temperature due to the associated pressure increase. This elevation can be described by the Clausius-Clapeyron relation modified to include the Laplace effect as given in Equation 4. [47]

$$T_1 = \left[\frac{1}{T_0} - \frac{R}{M_w \Delta_{vap} H} \ln\left(1 + \frac{2\sigma}{r_d P_0}\right)\right]^{-1} \tag{4}$$

Where T_1 is the elevated boiling temperature, T_0 is boiling point (271.4K) at atmospheric pressure P_0 (101.3 kPa), M_w is molecular weight of PFB (238.03 g/mol) , $\Delta_{vap}H$ is enthalpy of vaporisation (100 kJ/mol), σ is surface tension and r_d is droplet radius.

The predicted elevated boiling temperature for PFB particles of varying diameter is shown in Figure 7a for surface tensions ranging from 5 – 20 mN/m, covering expected values for fluorocarbon droplets and bubbles [49]. For PFB particles at room temperature with diameters between 100 - 200 nm the majority lie below the vaporisation curve and would be expected to exist as liquid droplets. Previous work in our group has also shown that our NB sample experiences a rapid increase in size, measured via Dynamic Light Scattering, when heated above a threshold temperature of 57 °C suggesting the occurrence of a phase transition from liquid to gas. [27] This transition temperature matches closely to the predicted value in Figure 7a for a surface tensions of 10-15 mN/m. Additionally, we see that the predicted vaporisation
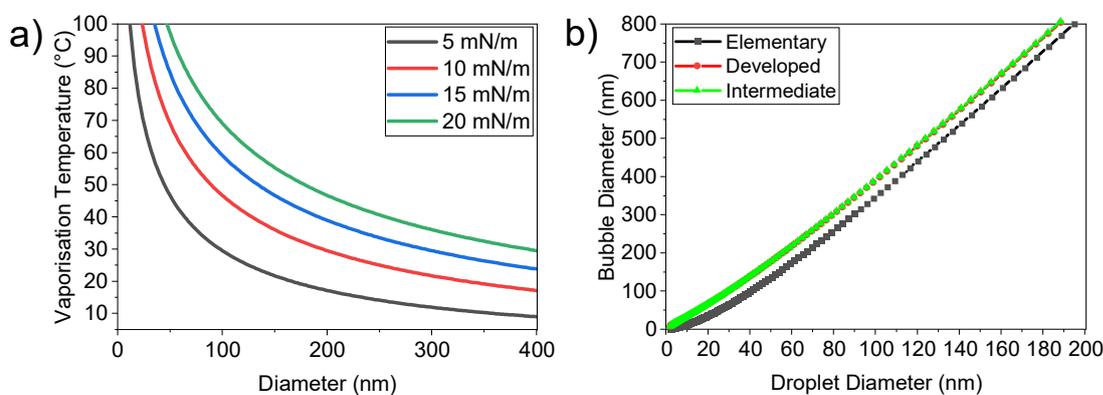
Figure 7. (a) Vaporisation temperature of a PFB droplet with varying surface tension calculated using the Clausius-Clapeyron relationship (Equation 4). (b) Predicted final bubble diameter after vaporisation of a PFB droplet comparing 3 models documented from [48].

temperature for these values lie within the range of temperatures measured during our CW HIFU release exposures (Figure S5), supporting the hypothesis of a phase-change release trigger.

To determine whether droplet vaporisation would be capable of inducing liposomal drug release, a model developed by *Evans et al* [48] was used to predict the expected diameter increase of the resultant bubble post vaporisation. There are 3 models with increasing complexity, which we have labelled as elementary, developed and intermediate. Briefly, the developed model accounts for a change in solubility of the core after vaporisation, whereas the elementary model neglects this. The intermediate model adds additional complexity by assuming partial equilibration of the core with a surrounding region around the particle. The predicted bubble size post-vaporisation is shown in Figure 7b for all three models, assuming a droplet surface tension $\sigma_d = 10 \text{ mN/m}$ and bubble surface tension $\sigma_b = 20 \text{ mN/m}$. For droplets of $100 - 200$ nm diameter, all models produced similar results with expected bubble diameter post vaporisation of > 300 nm, i.e. larger than the modal size of our encapsulating liposomes, which suggests that this expansion is capable of release the encapsulated payload.

4   Conclusion

This study demonstrated the diagnostic and therapeutic potential of Nested-NBs. Perfluorobutane NBs were co-loaded with model-drug into liposomes less than 300nm in diameter. The resultant Nested-NBs displayed good echogenicity at clinically relevant imaging frequencies (3-8 MHz). Triggered release was investigated using continuous and pulsed HIFU. Pulsed HIFU led to NB destruction but did not lead to significant drug release. In contrast, continuous-wave HIFU produced drug release across a range of PNPs. We can understand our observations if, at room temperature, our Nested-NBs contain a mix of both encapsulated PFB

NBs and PFB droplets. During continuous wave HIFU the sample temperature was also found to increase above a predicted threshold such that the PFB droplets underwent a phase-change from the liquid to gas state. The subsequent increase their diameter, by a factor of 3, led to liposome rupture and drug release. Thus Nested-NBs have both diagnostic potential, providing contrast enhancement for clinically relevant ultrasound frequencies, as well as the ability to trigger drug release through a the vaporisation of PFB droplets.

ASSOCIATED CONTENT

Supporting Information. The Supporting Information is available free of charge on the ACS Publications website at DOI: 10.XXX/acsami.XXXXXXX.

Resonant mass measurements of NB populations before and after HIFU; Change in B-mode intensity after cleaning of Nested-NBs; NTA populations and TEM images before and after cleaning of Nested-NBs; Broadband and Harmonic emissions for total duration of HIFU exposure for Nested-NBs, Liposomes and PBS; Maximum sample temperature measured during HIFU exposure. (PDF)

AUTHOR INFORMATION

Corresponding Author

- Tel./Fax : (+44) (0)113 343 3852. E-mail: S.D.Evans@leeds.ac.uk

Author Contributions

D.V.B.B. performed research, analyzed data and wrote the manuscript. J.R.M. assisted with experimental procedure for HIFU and PCD experiments including analysis tools. R.H.A, P.L.C.,

S.A.P., J.R.M. and S.D.E. helped to design the experimental plan, analyze data and write the manuscript.

REFERENCES

(1)   Shapiro, C. L.; Recht, A. Side Effects of Adjuvant Treatment of Breast Cancer. *N. Engl. J. Med.* **2001**, *344* (26), 1997–2008. https://doi.org/10.1056/NEJM200106283442607.

(2)   Luo, R.; Li, Y.; He, M.; Zhang, H.; Yuan, H.; Johnson, M.; Palmisano, M.; Zhou, S.; Sun, D. Distinct Biodistribution of Doxorubicin and the Altered Dispositions Mediated by Different Liposomal Formulations. *Int. J. Pharm.* **2017**, *519* (1–2), 1–10. https://doi.org/10.1016/j.ijpharm.2017.01.002.

(3)   Klibanov, A. L.; Shevchenko, T. I.; Raju, B. I.; Seip, R.; Chin, C. T. Ultrasound-Triggered

Release of Materials Entrapped in Microbubble-Liposome Constructs: A Tool for Targeted Drug Delivery. *J. Control. Release* **2010**, *148* (1), 13–17. https://doi.org/10.1016/j.jconrel.2010.07.115.

(4)   Wu, G.; Zasadzinski, J. A.; Mikhailovsky, A.; Khant, H. A.; Fu, C.; Chiu, W. Remotely Triggered Liposome Release by Near-Infrared Light Absorption via Hollow Gold Nanoshells. *J. Am. Chem. Soc.* **2008**, *130* (26), 8175–8177. https://doi.org/10.1021/ja802656d.

(5)   Kok, M. P.; Segers, T.; Versluis, M. Bubble Sorting in Pinched Microchannels for Ultrasound Contrast Agent Enrichment. *Lab Chip* **2015**, *15* (18), 3716–3722. https://doi.org/10.1039/c5lc00370a.

(6)   Owen, J.; Grove, P.; Rademeyer, P.; Stride, E.; Owen, J.; Grove, P.; Rademeyer, P.; Stride, E. The Influence of Blood on Targeted Microbubbles. *J. R. Soc Interface* **2014**, *11:2014062*.

(7)   Sirsi, S. R.; Borden, M. A. Microbubble Compositions, Properties and Biomedical Applications. *Bubble Sci. Eng. Technol.* **2009**, *1* (1–2), 3–17. https://doi.org/10.1179/175889709X446507.

(8)   Lee, M.; Lee, E. Y.; Lee, D.; Park, B. J. Stabilization and Fabrication of Microbubbles: Applications for Medical Purposes and Functional Materials. *Soft Matter* **2015**, *11* (11), 2067–2079. https://doi.org/10.1039/C5SM00113G.

(9)   van Rooij, T.; Skachkov, I.; Beekers, I.; Lattwein, K. R.; Voorneveld, J. D.; Kokhuis, T. J. A.; Bera, D.; Luan, Y.; van der Steen, A. F. W.; de Jong, N.; Kooiman, K. Viability of

Endothelial Cells after Ultrasound-Mediated Sonoporation: Influence of Targeting, Oscillation, and Displacement of Microbubbles. *J. Control. Release* **2016**, *238*, 197–211. https://doi.org/10.1016/j.jconrel.2016.07.037.

(10)   Kooiman, K.; Vos, H. J.; Versluis, M.; De Jong, N. Acoustic Behavior of Microbubbles and Implications for Drug Delivery. *Advanced Drug Delivery Reviews*. 2014, pp 28–48. https://doi.org/10.1016/j.addr.2014.03.003.

(11)   Browning, R.; Stride, E. Microbubble-Mediated Delivery for Cancer Therapy. *Fluids* **2018**, *3* (4), 74. https://doi.org/10.3390/fluids3040074.

(12)   Kooiman, K.; Foppen-Harteveld, M.; Der Steen, A. F. W. Van; De Jong, N. Sonoporation of Endothelial Cells by Vibrating Targeted Microbubbles. *J. Control. Release* **2011**, *154* (1), 35–41. https://doi.org/10.1016/j.jconrel.2011.04.008.

(13)   Lentacker, I.; De Cock, I.; Deckers, R.; De Smedt, S. C.; Moonen, C. T. W. Understanding Ultrasound Induced Sonoporation: Definitions and Underlying Mechanisms. *Adv. Drug Deliv. Rev.* **2014**, *72*, 49–64. https://doi.org/10.1016/j.addr.2013.11.008.

(14)   McLaughlan, J.; Ingram, N.; Smith, P. R.; Harput, S.; Coletta, P. L.; Evans, S.; Freear, S. Increasing the Sonoporation Efficiency of Targeted Polydisperse Microbubble Populations Using Chirp Excitation. *IEEE Trans. Ultrason. Ferroelectr. Freq. Control* **2013**, *60* (12), 2511–2520. https://doi.org/10.1109/TUFFC.2013.2850.

(15)   Fix, S. M.; Borden, M. A.; Dayton, P. A. Therapeutic Gas Delivery via Microbubbles and Liposomes. *J. Control. Release* **2015**, *209*, 139–149.

https://doi.org/10.1016/j.jconrel.2015.04.027.

(16)   Nesbitt, H.; Sheng, Y.; Kamila, S.; Logan, K.; Thomas, K.; Callan, B.; Taylor, M. A.; Love, M.; O'Rourke, D.; Kelly, P.; Beguin, E.; Stride, E.; McHale, A. P.; Callan, J. F. Gemcitabine Loaded Microbubbles for Targeted Chemo-Sonodynamic Therapy of Pancreatic Cancer. *J. Control. Release* **2018**, *279* (April), 8–16. https://doi.org/10.1016/j.jconrel.2018.04.018.

(17)   Peyman, S. A.; Abou-Saleh, R. H.; McLaughlan, J. R.; Ingram, N.; Johnson, B. R. G.; Critchley, K.; Freear, S.; Evans, J. A.; Markham, A. F.; Coletta, P. L.; Evans, S. D. Expanding 3D Geometry for Enhanced On-Chip Microbubble Production and Single Step Formation of Liposome Modified Microbubbles. *Lab Chip* **2012**, *12* (21), 4544. https://doi.org/10.1039/c2lc40634a.

(18)   Malik, R.; Pancholi, K.; Melzer, A. Microbubble–Liposome Conjugate: Payload Evaluation of Potential Theranostic Vehicle. *Nanobiomedicine* **2016**, *3*, 1–8. https://doi.org/10.1177/1849543516670806.

(19)   Yan, F.; Li, L.; Deng, Z.; Jin, Q.; Chen, J.; Yang, W.; Yeh, C. K.; Wu, J.; Shandas, R.; Liu, X.; Zheng, H. Paclitaxel-Liposome-Microbubble Complexes as Ultrasound-Triggered Therapeutic Drug Delivery Carriers. *J. Control. Release* **2013**, *166* (3), 246–255. https://doi.org/10.1016/j.jconrel.2012.12.025.

(20)   Neoh, K. G.; Kang, E. T. Functionalization of Inorganic Nanoparticles with Polymers for Stealth Biomedical Applications. *Polym. Chem.* **2011**, *2* (4), 747–759. https://doi.org/10.1039/c0py00266f.

(21)   Greish, K. Enhanced Permeability and Retention (EPR) Effect for Anticancer Nanomedicine Drug Targeting. In *Cancer Nanotechnology: Methods and Protocols*; Grobmyer, S. R., Moudgil, B. M., Eds.; Humana Press: Totowa, NJ, 2010; pp 25–37. https://doi.org/10.1007/978-1-60761-609-2_3.

(22)   Maeda, H. The Enhanced Permeability and Retention (EPR) Effect in Tumor Vasculature: The Key Role of Tumor-Selective Macromolecular Drug Targeting. *Adv. Enzyme Regul.* **2001**, *41* (1), 189–207. https://doi.org/10.1016/S0065-2571(00)00013-3.

(23)   Bosca, F.; Bielecki, P. A.; Exner, A. A.; Barge, A. Porphyrin-Loaded Pluronic Nanobubbles: A New US-Activated Agent for Future Theranostic Applications. *Bioconjug. Chem.* **2018**, *29* (2), 234–240. https://doi.org/10.1021/acs.bioconjchem.7b00732.

(24)   Wang, L.; Zhang, M.; Tan, K.; Guo, Y.; Tong, H.; Fan, X.; Fang, K. Preparation of Nanobubbles Carrying Androgen Receptor SiRNA and Their Inhibitory Effects on Androgen-Independent Prostate Cancer When Combined with Ultrasonic Irradiation. *PLoS One* **2014**, *9* (5). https://doi.org/10.1371/journal.pone.0096586.

(25)   Wu, H.; Abenojar, E. C.; Perera, R.; De Leon, A. C.; An, T.; Exner, A. A. Time-Intensity-Curve Analysis and Tumor Extravasation of Nanobubble Ultrasound Contrast Agents. *Ultrasound Med. Biol.* **2019**, *45* (9), 2502–2514. https://doi.org/10.1016/j.ultrasmedbio.2019.05.025.

(26)   Nittayacharn, P.; Yuan, H.-X.; Hernandez, C.; Bielecki, P.; Zhou, H.; Exner, A. A. Enhancing Tumor Drug Distribution with Ultrasound-Triggered Nanobubbles. *J. Pharm.*

Sci. **2019**, 1–8. https://doi.org/10.1016/j.xphs.2019.05.004.

(27) Peyman, S. A.; McLaughlan, J. R.; Abou-Saleh, R. H.; Marston, G.; Johnson, B. R. G.; Freear, S.; Coletta, P. L.; Markham, A. F.; Evans, S. D. On-Chip Preparation of Nanoscale Contrast Agents towards High-Resolution Ultrasound Imaging. *Lab Chip* **2016**, *16* (4), 679–687. https://doi.org/10.1039/C5LC01394A.

(28) Xing, Z.; Wang, J.; Ke, H.; Zhao, B.; Yue, X. The Fabrication of Novel Nanobubble Ultrasound Contrast Agent for Potential Tumor Imaging. **2010**. https://doi.org/10.1088/0957-4484/21/14/145607.

(29) Wu, M.; Zhao, H.; Guo, L.; Wang, Y.; Song, J.; Zhao, X.; Li, C.; Hao, L.; Wang, D.; Tang, J. Ultrasound-Mediated Nanobubble Destruction (UMND) Facilitates the Delivery of A10-3.2 Aptamer Targeted and SiRNA-Loaded Cationic Nanobubbles for Therapy of Prostate Cancer. *Drug Deliv.* **2018**, *25* (1), 226–240. https://doi.org/10.1080/10717544.2017.1422300.

(30) Chandan, R.; Banerjee, R. Pro-Apoptotic Liposomes-Nanobubble Conjugate Synergistic with Paclitaxel: A Platform for Ultrasound Responsive Image-Guided Drug Delivery. *Sci. Rep.* **2018**, *8* (1), 1–15. https://doi.org/10.1038/s41598-018-21084-8.

(31) Alheshibri, M.; Qian, J.; Jehannin, M.; Craig, V. S. J. A History of Nanobubbles. *Langmuir* **2016**, *32* (43), 11086–11100. https://doi.org/10.1021/acs.langmuir.6b02489.

(32) Nirmalkar, N.; Pacek, A. W.; Barigou, M. On the Existence and Stability of Bulk Nanobubbles. *Langmuir* **2018**, *34*, 10964–10973. https://doi.org/10.1021/acs.langmuir.8b01163.

(33) Perera, R. H.; Wu, H.; Peiris, P.; Hernandez, C.; Burke, A.; Zhang, H.; Exner, A. A. Improving Performance of Nanoscale Ultrasound Contrast Agents Using N,N-Diethylacrylamide Stabilization. *Nanomedicine Nanotechnology, Biol. Med.* **2017**, *13* (1), 59–67. https://doi.org/10.1016/j.nano.2016.08.020.

(34) Hernandez, C.; Abenojar, E. C.; Hadley, J.; De Leon, A. C.; Coyne, R.; Perera, R.; Gopalakrishnan, R.; Basilion, J. P.; Kolios, M. C.; Exner, A. A. Sink or Float? Characterization of Shell-Stabilized Bulk Nanobubbles Using a Resonant Mass Measurement Technique. *Nanoscale* **2019**, *11* (3), 851–855. https://doi.org/10.1039/c8nr08763f.

(35) Tan, B. H.; An, H.; Ohl, C.-D. How Bulk Nanobubbles Might Survive. *Phys. Rev. Lett.* **2020**, *124* (13), 134503. https://doi.org/10.1103/physrevlett.124.134503.

(36) Hernandez, C.; Nieves, L.; De Leon, A. C.; Advincula, R.; Exner, A. A. Role of Surface Tension in Gas Nanobubble Stability under Ultrasound. *ACS Appl. Mater. Interfaces* **2018**, *10* (12), 9949–9956. https://doi.org/10.1021/acsami.7b19755.

(37) Pellow, C.; Acconcia, C.; Zheng, G.; Goertz, D. E. Threshold-Dependent Nonlinear Scattering from Porphyrin Nanobubbles for Vascular and Extravascular Applications. *Phys. Med. Biol.* **2018**, *63* (21). https://doi.org/10.1088/1361-6560/aae571.

(38) JafariSojahrood, A.; Nieves, L.; Hernandez, C.; Exner, A.; Kolios, M. C. Theoretical and Experimental Investigation of the Nonlinear Dynamics of Nanobubbles Excited at Clinically Relevant Ultrasound Frequencies and Pressures: The Role Oflipid Shell Buckling. **2017**, No. December, 6–9.

(39)   Cavalli, R.; Bisazza, A.; Trotta, M.; Argenziano, M.; Civra, A.; Donalisio, M.; Lembo, D.
New Chitosan Nanobubbles for Ultrasound-Mediated Gene Delivery: Preparation and in
Vitro   Characterization.   *Int.   J.   Nanomedicine*   **2012**,   *7*,   3309–3318.
https://doi.org/10.2147/IJN.S30912.

(40)   Nguyen, A. T.; Wrenn, S. P. Acoustically Active Liposome-Nanobubble Complexes for
Enhanced Ultrasonic Imaging and Ultrasound-Triggered Drug Delivery. *Wiley Interdiscip.
Rev.   Nanomedicine   Nanobiotechnology*   **2014**,   *6*   (3),   316–325.
https://doi.org/10.1002/wnan.1255.

(41)   Zhu, L. Preparation Of Nanobubbles Modified With A Small-Molecule CXCR4
Antagonist For Targeted Drug Delivery To Tumors And Enhanced Ultrasound Molecular
Imaging. **2019**. https://doi.org/10.2147/IJN.S210478.

(42)   Ruckenstein, E. Nanodispersions of Bubbles and Oil Drops in Water. *Colloids Surfaces A
Physicochem.   Eng.   Asp.*   **2013**,   *423*,   112–114.
https://doi.org/10.1016/j.colsurfa.2013.01.056.

(43)   Abenojar, E. C.; Nittayacharn, P.; De Leon, A. C.; Perera, R.; Wang, Y.; Bederman, I.;
Exner, A. A. Effect of Bubble Concentration on the in Vitro and in Vivo Performance of
Highly Stable Lipid Shell-Stabilized Micro- and Nanoscale Ultrasound Contrast Agents.
Langmuir **2019**. https://doi.org/10.1021/acs.langmuir.9b00462.

(44)   Nie, L.; McLaughlan, J. R.; Cowell, D. M. J.; Carpenter, T. M.; Freear, S. Subharmonic
Plane Wave Imaging of Liposome-Loaded Microbubbles. *IEEE Int. Ultrason. Symp. IUS*
2018, *2018-Janua*. https://doi.org/10.1109/ULTSYM.2018.8580201.

(45)   McLaughlan, J. R.; Cowell, D. M. J.; Freear, S. Gold Nanoparticle Nucleated Cavitation for Enhanced High Intensity Focused Ultrasound Therapy. *Phys. Med. Biol.* **2018**, *63* (1). https://doi.org/10.1088/1361-6560/aa97e9.

(46)   McLaughlan, J.; Rivens, I.; Leighton, T.; ter Haar, G. A Study of Bubble Activity Generated in Ex Vivo Tissue by High Intensity Focused Ultrasound. *Ultrasound Med. Biol.* **2010**, *36* (8), 1327–1344. https://doi.org/10.1016/j.ultrasmedbio.2010.05.011.

(47)   Doinikov, A. A.; Sheeran, P. S.; Bouakaz, A.; Dayton, P. A. Vaporisation Dynamics of Volatile Perfluorocarbon Droplets: A Theoretical Model and *in Vitro* Validation. *Med. Phys.* **2014**, *41* (10), 102901. https://doi.org/10.1118/1.4894804.

(48)   Evans, D. R.; Parsons, D. F.; Craig, V. S. J. Physical Properties of Phase-Change Emulsions. *Langmuir* **2006**, *22* (23), 9538–9545. https://doi.org/10.1021/la062097u.

(49)   Abou-Saleh, R. H.; Peyman, S. A.; Johnson, B. R. G.; Marston, G.; Ingram, N.; Bushby, R.; Coletta, P. L.; Markham, A. F.; Evans, S. D. The Influence of Intercalating Perfluorohexane into Lipid Shells on Nano and Microbubble Stability. *Soft Matter* **2016**, *12* (34), 7223–7230. https://doi.org/10.1039/C6SM00956E.